

From a fractional quantum anomalous Hall state to a smectic state with equal Hall conductance

Hongyu Lu,^{1,*} Han-Qing Wu,^{2,*} Bin-Bin Chen,¹ and Zi Yang Meng^{1,†}

¹*Department of Physics and HKU-UCAS Joint Institute of Theoretical and Computational Physics,
The University of Hong Kong, Pokfulam Road, Hong Kong SAR, China*

²*Guangdong Provincial Key Laboratory of Magnetoelectric Physics and Devices,
School of Physics, Sun Yat-sen University, Guangzhou 510275, China*

(Dated: May 20, 2024)

The recent developments in moiré materials have generated widespread attention to the general features of fractional quantum anomalous Hall (FQAH) states, including their possible coexistence with and transition to various symmetry breaking charge ordered states. These attentions are pushing forward our knowledge of the relation between the topological order in FQAH states and the Landau-type of symmetry breaking order such as the 1D smectic electronic liquid crystal and 2D charge-density-wave (CDW) solid. Although the transitions from topological states to symmetry breaking states with trivial topology have been discussed, the road from one topological ordered state to another with equal Hall conductance and broken translational symmetry has not been found. Here we show the intriguing evidence that the FQAH to FQAH Smectic (FQAHS) transition is robustly realizable in the archetypal correlated flat Chern-band model at filling $\nu = 2/3$. This transition is novel in that: i) the FQAHS acquires the same fractional Hall conductance as FQAH, which cannot be explained by mean-field band folding. The formation of smectic order can be viewed as perturbation around the transition point, and thus, do not destroy or change the original topology; ii) the charge excitation remains gapped across the transition although the neutral gap is closed at transition point; and iii) the transition is triggered by the softening of roton mode with the same wave vector as the smectic order. Our discovery opens countless new possibilities, both theoretical and experimental, in the fast-growing field of robust fractional Chern insulators.

Introduction.— The interplay between Landau-type symmetry breaking order such as 1D smectic electronic liquid crystal and 2D charge-density-wave (CDW) solid [1, 2] and topological order such as fractional quantum Hall (FQH) [3–22] and fractional quantum anomalous Hall/Chern insulator (FQAH/FCI) [23–40], has been a focal point in theories and experiments in past several decades. Such interplay usually manifest in two forms – the transition between and the coexistence of – topological order and Landau-type charge order.

The phase transition between FQH or FQAH and charge density waves (CDW) is better understood [15–19, 21–30, 34, 38, 39, 41–45]. In the Landau-level systems, as the magnetoroton modes are identified as the elementary low-energy collective excitations in FQH states [9, 46–53], the possible transitions via softening such modes are widely discussed [15–18, 22]. In the isotropic Landau levels, the softening of roton modes inevitably leads to first-order transitions [54], due to the presence of cubic term in the free energy [55] and the negative sign of the vertex function from critical fluctuations. However, artificially tuning the band mass anisotropy can lead to a possible continuous transition from a $2 + 1/3$ FQH state to a stripe state [22]. Besides, in the absence of magnetic field, a possible continuous transition from a FQAH state to a CDW metal state with spontaneously translational symmetry breaking driven by the roton condensation has been reported as well [39], suggesting the connection between FQH and FQAH in their response to the collective roton excitations.

The coexistence of topological order and charge order has been proposed for long time as well [3–8, 33]. In the Landau-level systems, to the best of our knowledge, only the coexistence of FQH with nematic order (breaks the rotational symmetry while conserves translational symmetry) has been identified [6, 10–14, 20, 21, 56]. Such realization turns to

be more versatile in zero-field Chern insulators. One exotic type is the coexisting CDW order to fold the Chern band, and thus result in anomalous Hall crystals (AHC) with Hall conductivity in the unit of e^2/h different from the Chern number of the underlying band multiplied by the filling factor: $\sigma_{xy} \neq \nu C_{\text{band}}$ [29]. Such a QAHC state with integer σ_{xy} at fractional filling of a $|C| = 1$ band has been numerically computed in the continuum model for tMoTe₂ bilayers at $\nu = 1/2$ [38] and predicted in AB-Stacked MoTe₂/WSe₂ at $\nu = 2/3$ via mean-field analysis [35]. FQAHC states with $\sigma_{xy} \neq \nu C_{\text{band}}$ have also been simulated in lattice models [31, 32], where only part of the particles form the CDW while the remaining part contribute to the topology. Another realization of AHC states has been reported in the mean-field studies of rhombohedral multilayer graphene systems, where a crystal band with non-trivial topology $|C| = 1$ is driven by interaction [41–45], although the role of moiré potential therein is still under debate.

Moreover, in the lattice model, a FQAH state coexisting with a 1D smectic charge order (FQAHS) has been reported with numerical evidence [40], where the Hall conductivity in the unit of e^2/h is equal to the fractional filling of the $C = 1$ Chern band: $\sigma_{xy} = \nu = 2/3$, while the ground-state degeneracy of the FQAH state is enhanced due to the translational symmetry breaking.

Experimentally, possible symmetry-breaking Chern insulators are only observed under finite magnetic field with integer σ_{xy} in twisted graphene systems [57, 58], followed by theoretical studies for more possibilities [36, 37]. However, despite of these discoveries and the fact that there have been significant advances in the realization of FQAH states recently [59–66], (F)QAHC states, as the coexistence of topological order and charge order, have not been found in experiments yet.

Since the transitions from FQAH to CDW states are well studied and the coexisting QAHC states are being intensively discussed, a natural and novel question would be the phase transition between the topological states with preserved and spontaneously broken translational symmetry. Although the transition between the composite Fermi liquid state and the interger $\sigma_{xy} = \frac{e^2}{h}$ AHC state at $\nu = 1/2$ has been numerically verified in the continuum model of tMoTe₂ [38], to the best of our knowledge, there exists no discovery of a direct transition from a FQAH state to a translational symmetry breaking state *with the same Hall conductance*. Even in the better-understood Landau-level systems, only the transitions between isotropic and nematic FQH states (with the same Hall conductance while breaking only rotational symmetry) are identified [10, 11, 20, 21, 56], while the transition between an isotropic FQH state and a FQH state with broken translational symmetry has not been reported. Fortunately, in previous studies, the $C = 2/3$ FQAH and FQAHS states are discovered in the same model with the same filling factor [39, 40], which hint the existence of a direct transition from FQAH to FQHAS in the rich phase space of the model.

In this work, we find this direct transition from the $C = 2/3$ FQAH state to the $C = 2/3$ FQAHS state by numerically studying the flat Chern-band model on checkerboard lattice with $\nu = 2/3$ filling of the flat band [39, 40, 67–71], using exact diagonalizations (ED) and density matrix renormalization group (DMRG) methods to navigate in the global phase diagram. This novel transition exhibits the following distinct features: i) the FQAHS has the same fractional Hall conductance as FQAH, which cannot be explained by mean-field band folding, while the formation of the smectic order could be taken as a perturbation around the critical point, without destroying or changing the original topological order; ii) at the critical point between the FQAH and FQAHS, although the neutral excitation gap is closed, the charge excitation remains gapped; iii) the smectic order is induced from the softening of the roton mode. Deep in the FQAH state, the roton minima is at (π, π) , while the roton mode at $(\pi, 0)$ goes soft, becomes the lowest mode towards the transition point, and finally condenses when the $(\pi, 0)$ smectic order is established. After the transition, when deep in the FQAHS state, the roton minima is found at $(0, \pi)$, different from the wave vector of charge order. Therefore, our work establishes a new perspective in the symmetry-breaking transitions between FQAH states, and such a transition with distinct features might be observed in future experiments.

Model and methods.— We consider the $\nu = 2/3$ filling of the flat band with spinless fermions on the checkerboard lattice [39, 40],

$$\begin{aligned}
 H = & - \sum_{\langle i,j \rangle} t e^{i\phi_{ij}} (c_i^\dagger c_j + h.c.) - \sum_{\langle\langle i,j \rangle\rangle} t'_{ij} (c_i^\dagger c_j + h.c.) \\
 & - \sum_{\langle\langle\langle i,j \rangle\rangle\rangle} t'' (c_i^\dagger c_j + h.c.) + \sum_{i,j} V(n_i - \frac{1}{2})(n_j - \frac{1}{2}),
 \end{aligned} \tag{1}$$

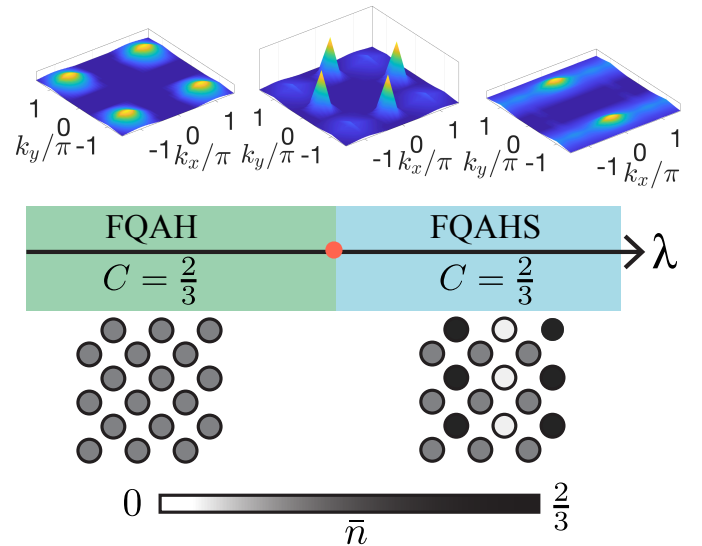


FIG. 1. Direct FQAH-FQAHS transition. The two phases both acquire the same Chern number $C = 2/3$. The orange dot in the phase diagram refers to the direct transition point. For the studied path in the main text ($V_1 = 1.5(1 - \lambda)$, $V_2 = 1$, and $V_3 = 1.5\lambda$), the critical point is $\lambda_c \approx 0.338$ from the DMRG results. In the upper panel, we show the density structure factors $S(\mathbf{q})$. The one describing the critical point is schematic while the other two are numerically obtained in a $N_y = 6$ cylinder. In the FQAH state, the roton minimum is at (π, π) , when approaching the critical point, the $(\pi, 0)$ and $(0, \pi)$ modes go soft. Then the $(\pi, 0)$ mode condenses and forms the smectic order, while the re-opened roton gap is at $(0, \pi)$. In the lower panel, we show the schematic real-space electron density distributions. The electrons in the FQAH state are uniformly distributed, while the translation symmetry is spontaneously broken in FQAHS state, and there exists a $(\pi, 0)$ smectic order in one sublattice.

with $t = 1$ (as the energy unit), $t'_{ij} = \pm 1/(2 + \sqrt{2})$ with alternating sign in edge-sharing plaquettes, $t'' = -1/(2 + 2\sqrt{2})$ and $\phi_{ij} = \frac{\pi}{4}$. We consider the nearest-neighbor (NN) interaction V_1 , the next-nearest-neighbor (NNN) interaction V_2 , and the next to next nearest-neighbor (NNNN) interaction V_3 .

The total number of lattice sites $N = N_y \times N_x \times 2$, the average density \bar{n} and the filling of the flat band ν are defined as $\bar{n} = N_e/N = \nu/2$. Our DMRG simulations mainly utilize $3 \times 18 \times 2$ cylinders for the two-site unit cells with $L_y = 2N_y = 6$ legs in the periodic direction to study the transition, and $L_y = 12$ systems are considered in studying the two phases. The DMRG simulations are based on the QS-space library [72] with charge U(1) symmetry and complex wavefunctions. We keep the maximum bond dimension up to $D = 3444$ with truncation error $\epsilon < 10^{-10}$. The ED simulations are conducted in $3 \times 4 \times 2$ and $3 \times 6 \times 2$ tori.

The FQAH-FQAHS transition.— To study the transition in the global three-dimensional parameter space, we define a parameter λ such that V_1 , V_2 and V_3 interactions are functions of λ . In the main text, unless specified, we focus on the path $V_1 = 1.5(1 - \lambda)$, $V_2 = 1$, and $V_3 = 1.5\lambda$. The phase diagram

is shown in Fig. 1, and the critical point for the default path is $\lambda_c \approx 0.338$ from DMRG results. As discussed in the previous works [39, 40], the $C = 2/3$ FQAH state has uniform electron distribution and the roton minimum is at (π, π) . While the roton minimum of the $C = 2/3$ FQAH state with the smectic order in one sublattice is at $(0, \pi)$ (if the order is at $(\pi, 0)$). For better demonstration, we define the structure factor as $S(\mathbf{q}) = \sum_j e^{-i\mathbf{q}(\mathbf{r}_0 - \mathbf{r}_j)} (\langle n_0 n_j \rangle - \langle n_0 \rangle \langle n_j \rangle)$ by taking the Fourier transformation of density-density correlations, and the smectic order of the ordered sublattice (if not specified) as $\delta_{\text{smectic}} = \frac{2}{N'} \sum_i' (-1)^{x_i} n_{\mathbf{r}_i}$ with summation over a few unit cells i 's in the bulk and N' being the number of such sites. We show the structure factors of the two phases in the upper panel of Fig. 1, which are numerically obtained in a $6 \times 24 \times 2$ cylinder and in agreement with the previous works [39, 40].

We propose that this transition is driven by roton condensation and show the schematic $S(\mathbf{q})$ around the transition point in Fig. 1. When approaching the critical point, the $(\pi, 0)$ and $(0, \pi)$ modes both go soft due to the C_4 rotational symmetry in the FQAH state. Although the smectic order of FQAH state in the two directions are degenerate in the thermodynamic limit, our DMRG simulations would pick one direction ($(\pi, 0)$ here for example), and thus, the $(\pi, 0)$ mode condenses and smectic order forms, while the minimal roton gap at $(0, \pi)$ is opened again. We show the detailed ED and DMRG results of this transition in Figs. 2 and 3, respectively.

In Fig. 2 (a,b), the momentum sectors of the utilized $3 \times 4 \times 2$ and $3 \times 6 \times 2$ tori in the Brillouin zone of the two-site unit cells are shown, where those containing the ground state sectors are marked with dark/light green/blue color, while the others are in gray. The energy spectrum from $\lambda = 0$ to $\lambda = 1$ with periodic boundary conditions of the two tori are shown in Fig. 2 (c,d), and the definitions of the colors here are the same as in Fig. 2 (a,b). In the $3 \times 4 \times 2$ case, when λ is small, the 3-fold ground states of the FQAH state are from $(0, 0)$ and $(0, \pm \frac{2\pi}{3})$ sectors, while those in the $3 \times 6 \times 2$ case are all from the $(0, 0)$ sector. When approaching the critical point and in the process of forming the smectic order, there are another three states from $(\pi, 0)$ and $(\pi, \pm \frac{2\pi}{3})$ sectors in the $3 \times 4 \times 2$ case and all from the $(\pi, 0)$ sectors in the $3 \times 6 \times 2$ case, merging into the original ground states. Therefore, there exists 6-fold degeneracy in the FQAH ground states, and we show the energy spectra of a $3 \times 4 \times 2$ torus with twisted boundary conditions at $\lambda = 0.2, 0.4$, in Fig. 2 (e,f). In the thermodynamic limit, the ground-state degeneracy should be 12 in the FQAH state, since the smectic orders in two directions are degenerate [40]. We see only 6-fold here due to the finite size effect, i.e. $(\pi, 0)$ and $(0, \pi)$ sectors do not exist simultaneously.

The charge gap defined as $\Delta_{\text{charge}} = E(N, N_e + 1) + E(N, N_e - 1) - 2E(N, N_e)$ in a $3 \times 4 \times 2$ torus as a function of λ is shown in Fig. 2 (g), which exhibits one of the unique features of the FQAH-FQAH transition that although the neutral excitation gap is closed at the critical point, the charge excitation remains gapped. The second derivatives of the ground state energy (taken from the state with lowest energy) as a

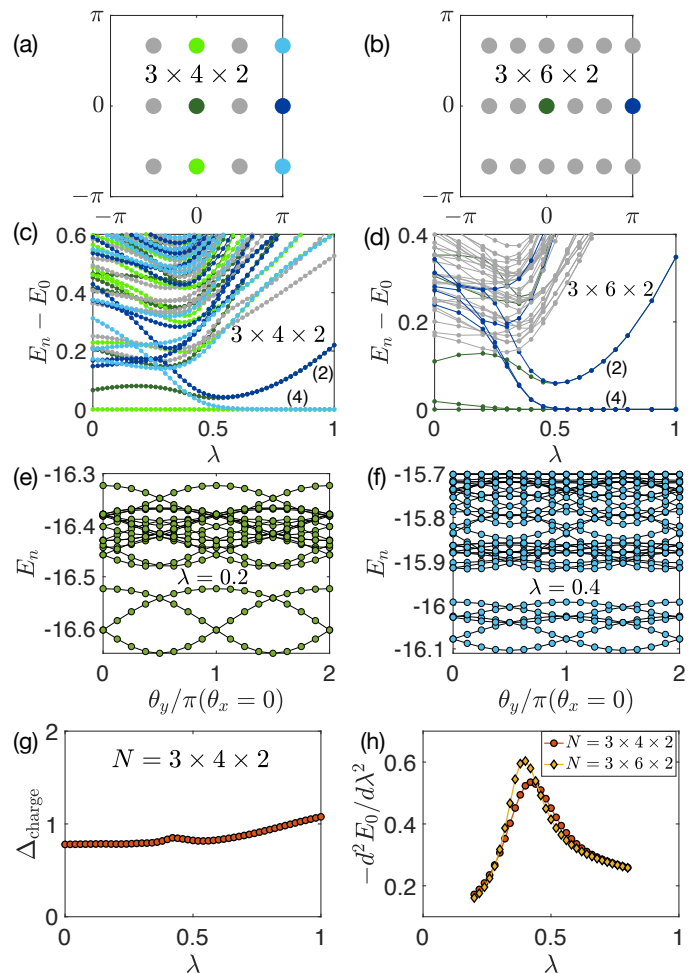


FIG. 2. ED results for the FQAH-FQAH transition. (a) and (b) show the Brillouin zone of $3 \times 4 \times 2$ torus and $3 \times 6 \times 2$ torus respectively. The momentum sectors related to the ground states are marked with light/dark green/blue colors, while the others are marked with gray. (c) and (d) show the energy spectra with the changing of λ for $3 \times 4 \times 2$ torus and $3 \times 6 \times 2$ torus respectively, and the colors represent the momentum sectors specified in (a) and (b). In the FQAH state, the number of fully degenerate states in periodic boundary conditions are labeled. (e) and (f) show the twisted energy spectrum at $\lambda = 0.2$ and $\lambda = 0.4$, respectively, exhibiting the 3-fold (6-fold) ground-state degeneracy of FQAH(S) state. The charge gap with the changing of λ for a $3 \times 4 \times 2$ torus is shown in (g). (h) The second derivative of ground state energy with respect to λ .

function of λ for the two system sizes are shown in Fig. 2 (h), which supports that this FQAH-FQAH transition is continuous, which can also be seen from the smooth merging of the ground states around the transition point in Fig. 2 (c) and (d).

Another important feature of this transition is that the Chern number of the FQAH state with 6-fold ground-state degeneracy here is also $C = 2/3$, the same as the FQAH state. This cannot be simply explained by mean-field band folding. Since the smectic order is $(\pi, 0)$, the folding of the Chern band will lead to a $1 + 1/3$ filling, and if still topologically non-trivial, the Chern number of the new state should be $1/3$, not con-

sistent with our measurements. However, the formation of the smectic order could be treated as a perturbation around the critical point, and thus it does not destroy or change the original topological order. In other words, the 3 new merging ground states (perturbation around transition point) also carry a Chern number $C = 2/3$ [73], while the mean-field band folding picture would refer to the situation that the Chern numbers of the 3 new ground states are 0.

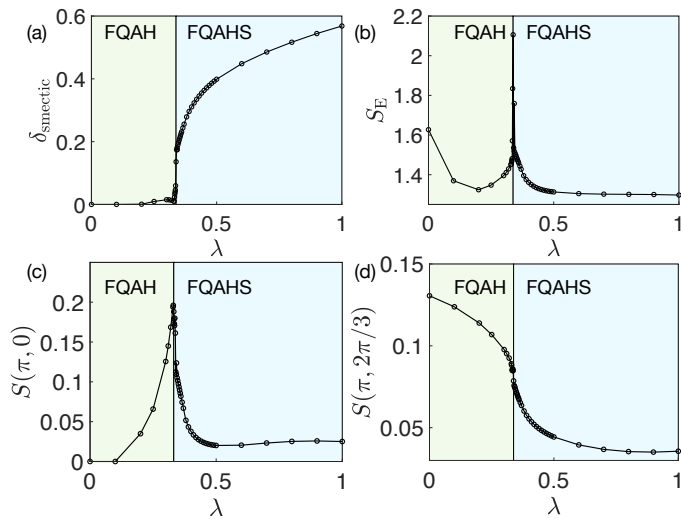


FIG. 3. **DMRG results for the FQAH-FQAHS transition.** The evolution of (a) smectic order parameter, (b) bipartite entanglement entropy, (c) $S(\pi, 0)$ and (d) $S(\pi, 2\pi/3)$ with the change of tuning parameter λ from a $L_y = 6$ cylinder. The critical point is $\lambda_c \approx 0.338$.

The DMRG results are shown in Fig. 3, including (a) the smectic order parameter, (b) the bipartite entanglement entropy, (c) change of $S(\pi, 0)$, and (d) change of $S(\pi, 2\pi/3)$. In the FQAH state, as shown in Fig. 1 and mentioned above, the roton minimum is at (π, π) . As we consider a $3 \times 18 \times 2$ cylinder here, we use the value of $S(\pi, 2\pi/3)$ to describe the evolution of the dispersive (π, π) mode (we find it hard for DMRG simulatinos of cylinders with larger width, when approaching the critical point). We also focus on the evolution of $(\pi, 0)$ mode along this transition, which is far from a low-energy mode when deep in the FQAH state (small λ). When approaching the critical point, the $(\pi, 0)$ mode gradually goes soft and becomes the lowest neutral excitation mode. At the critical point $\lambda_c \approx 0.338$, the value of $S(\pi, 0)$ (which represents the smectic susceptibility) goes to the peak and the mode condenses when the smectic order is formed and the bipartite entanglement entropy also shows a singular value. After that, the value of $S(\pi, 0)$ decreases. These results manifest that the formation of smectic order and the FQAH-FQAHS transition is driven by the softening of the roton mode. Since the C_4 rotation symmetry is conserved in the FQAH state, the $(0, \pi)$ and $(\pi, 0)$ modes should go soft together when approaching λ_c . Since the data quality is worse for cylinders with larger width and the $3 \times 18 \times 2$ cylinder used here does not cover the $(0, \pi)$

momentum sector, we plot the schematic plot of $S(\mathbf{q})$ around the transition as shown in the upper panel of Fig. 1, unlike the other two figures of $S(\mathbf{q})$ deep in the phases which are numerically obtained from $N_y = 6$ cylinders. We can tell from the $S(\mathbf{q})$ in the FQAHS that the roton minimum is at $(0, \pi)$ when the smectic order is at $(\pi, 0)$ [40]. This implies that at the critical point, when the $(\pi, 0)$ mode condenses, the re-opened and finally stabilized roton minimum is at $(0, \pi)$ in the FQAHS state.

While the continuous FQAH-FQAHS transition is supported by the ED result, it is hard for the criticality analysis from the current DMRG results along this path due to the difficult convergence around the critical point. However, the important feature, that the direct transition is triggered from the softening of roton mode with the same vector as the smectic order to be formed, is well exhibited by the present numerical results. We show more results along other paths of this transition in Supplemental Material (SM) [74].

Discussions.— In summary, we find a direct transition from a $C = 2/3$ FQAH state to a $C = 2/3$ FQAHS state, which provides distinct perspectives in the interplay of topological order and symmetry-broken order, including both their transition and coexistence. The Chern number of the FQAHS state cannot be explained by the mean-field band folding, and the smectic charge order is stabilized from a perturbation which does not destroy or change the topological order. This example shows in general that $\sigma_{xy} = \nu C_{\text{band}}$ does not exclude the possibility of the coexisting CDW order in FQAH states, therefore in experiments, whether there exists coexisting CDW with FQAH cannot be simply decided by the relation between the quantized Hall conductance and filling, but needs further experimental detection of the charge order from other probes such as scanning tunneling spectroscopy as well.

While the 1D smectic order of this FQAHS case is not commensurate with filling, whether another CDW order that is commensurate with the filling could be introduced as a perturbation and not changing the original Hall conductivity, together with possible criticality analysis of either case, would be an interesting direction for future exploration. Finally, our results conclude that the roton condensation in FQAH states can in general lead to two consequences: a compressible CDW metal state with closing charge gap [39], or an insulating FQAH+CDW state with charge gap not closing at critical point, as reported in this work.

Acknowledgments — We thank Kai Sun and Bo Yang for helpful discussions. HYL, BBC and ZYM acknowledge the support from the Research Grants Council (RGC) of Hong Kong Special Administrative Region of China (Project Nos. 17301721, AoE/P-701/20, 17309822, HKU C7037-22GF, 17302223), the ANR/RGC Joint Research Scheme sponsored by RGC of Hong Kong and French National Research Agency (Project No. A_HKU703/22), the GD-NSF (No. 2022A1515011007) and the HKU Seed Funding for Strategic Interdisciplinary Research. We thank HPC2021 system under the Information Technology Services and the Blackbody HPC system at the Department of Physics, Uni-

versity of Hong Kong, as well as the Beijing PARATERA Tech CO.,Ltd. (URL: <https://cloud.paratera.com>) for providing HPC resources that have contributed to the research results reported within this paper. H.Q. Wu acknowledge the support from Guangzhou Basic and Applied Basic Research Foundation (No. 202201011569). The ED calculations reported were performed on resources provided by the Guangdong Provincial Key Laboratory of Magnetoelectric Physics and Devices, No. 2022B1212010008.

* The two authors contributed equally to this work.

† zymeng@hku.hk

- [1] S. A. Kivelson, E. Fradkin, and V. J. Emery, *Nature* **393**, 550 (1998).
- [2] V. J. Emery, E. Fradkin, S. A. Kivelson, and T. C. Lubensky, *Phys. Rev. Lett.* **85**, 2160 (2000).
- [3] S. Kivelson, C. Kallin, D. P. Arovas, and J. R. Schrieffer, *Phys. Rev. Lett.* **56**, 873 (1986).
- [4] B. I. Halperin, Z. Tešanović, and F. Axel, *Phys. Rev. Lett.* **57**, 922 (1986).
- [5] Z. Tešanović, F. m. c. Axel, and B. I. Halperin, *Phys. Rev. B* **39**, 8525 (1989).
- [6] L. Balents, *Europhysics Letters* **33**, 291 (1996).
- [7] E. Fradkin and S. A. Kivelson, *Phys. Rev. B* **59**, 8065 (1999).
- [8] G. Murthy, *Phys. Rev. Lett.* **85**, 1954 (2000).
- [9] I. V. Kukushkin, J. H. Smet, V. W. Scarola, V. Umansky, and K. von Klitzing, *Science* **324**, 1044 (2009).
- [10] M. Mulligan, C. Nayak, and S. Kachru, *Phys. Rev. B* **82**, 085102 (2010).
- [11] J. Maciejko, B. Hsu, S. A. Kivelson, Y. Park, and S. L. Sondhi, *Phys. Rev. B* **88**, 125137 (2013).
- [12] J. Xia, J. P. Eisenstein, L. N. Pfeiffer, and K. W. West, *Nature Physics* **7**, 845 (2011).
- [13] Y. Liu, S. Hasdemir, M. Shayegan, L. N. Pfeiffer, K. W. West, and K. W. Baldwin, *Phys. Rev. B* **88**, 035307 (2013).
- [14] Y. You, G. Y. Cho, and E. Fradkin, *Phys. Rev. X* **4**, 041050 (2014).
- [15] T.-L. Ho, *Phys. Rev. Lett.* **87**, 060403 (2001).
- [16] N. R. Cooper, N. K. Wilkin, and J. M. F. Gunn, *Phys. Rev. Lett.* **87**, 120405 (2001).
- [17] S. Sinha and G. V. Shlyapnikov, *Phys. Rev. Lett.* **94**, 150401 (2005).
- [18] B. Mukherjee, A. Shaffer, P. B. Patel, Z. Yan, C. C. Wilson, V. Crépel, R. J. Fletcher, and M. Zwierlein, *Nature* **601**, 58 (2022).
- [19] B. Yang, Z. Papić, E. H. Rezayi, R. N. Bhatt, and F. D. M. Haldane, *Phys. Rev. B* **85**, 165318 (2012).
- [20] B. Yang, *Phys. Rev. Res.* **2**, 033362 (2020).
- [21] N. Regnault, J. Maciejko, S. A. Kivelson, and S. L. Sondhi, *Phys. Rev. B* **96**, 035150 (2017).
- [22] P. Kumar and R. N. Bhatt, *Phys. Rev. B* **106**, 115101 (2022).
- [23] Y.-F. Wang, Z.-C. Gu, C.-D. Gong, and D. N. Sheng, *Phys. Rev. Lett.* **107**, 146803 (2011).
- [24] W.-W. Luo, A.-L. He, Y. Zhou, Y.-F. Wang, and C.-D. Gong, *Phys. Rev. B* **102**, 155120 (2020).
- [25] M. Barkeshli, N. Y. Yao, and C. R. Laumann, *Phys. Rev. Lett.* **115**, 026802 (2015).
- [26] W. Zhu, S. S. Gong, and D. N. Sheng, *Phys. Rev. B* **94**, 035129 (2016).
- [27] V. Crépel and L. Fu, *Phys. Rev. B* **107**, L201109 (2023).
- [28] X.-Y. Song, Y.-H. Zhang, and T. Senthil, (2023), [arXiv:2308.10903 \[cond-mat.str-el\]](https://arxiv.org/abs/2308.10903).
- [29] X.-Y. Song, C.-M. Jian, L. Fu, and C. Xu, (2023), [arXiv:2310.11632 \[cond-mat.str-el\]](https://arxiv.org/abs/2310.11632).
- [30] A. P. Reddy, F. Alsallom, Y. Zhang, T. Devakul, and L. Fu, *Phys. Rev. B* **108**, 085117 (2023).
- [31] S. Kourtis and M. Daghofer, *Phys. Rev. Lett.* **113**, 216404 (2014).
- [32] S. Kourtis, *Phys. Rev. B* **97**, 085108 (2018).
- [33] R. Sohal, L. H. Santos, and E. Fradkin, *Phys. Rev. B* **97**, 125131 (2018).
- [34] N. Morales-Durán, J. Wang, G. R. Schleder, M. Angeli, Z. Zhu, E. Kaxiras, C. Repellin, and J. Cano, *Phys. Rev. Res.* **5**, L032022 (2023).
- [35] H. Pan, M. Xie, F. Wu, and S. Das Sarma, *Phys. Rev. Lett.* **129**, 056804 (2022).
- [36] P. Wilhelm, T. C. Lang, and A. M. Läuchli, *Phys. Rev. B* **103**, 125406 (2021).
- [37] P. H. Wilhelm, T. C. Lang, M. S. Scheurer, and A. M. Läuchli, *SciPost Phys.* **14**, 040 (2023).
- [38] D. N. Sheng, A. P. Reddy, A. Abouelkomsan, E. J. Bergholtz, and L. Fu, [arXiv e-prints](https://arxiv.org/abs/2402.17832), [arXiv:2402.17832 \(2024\)](https://arxiv.org/abs/2402.17832), [arXiv:2402.17832 \[cond-mat.mes-hall\]](https://arxiv.org/abs/2402.17832).
- [39] H. Lu, H.-Q. Wu, B.-B. Chen, K. Sun, and Z. Y. Meng, (2024), [arXiv:2403.03258 \[cond-mat.str-el\]](https://arxiv.org/abs/2403.03258).
- [40] H. Lu, H.-Q. Wu, B.-B. Chen, K. Sun, and Z. Y. Meng, (2024), [arXiv:2401.00363 \[cond-mat.str-el\]](https://arxiv.org/abs/2401.00363).
- [41] B. Zhou, H. Yang, and Y.-H. Zhang, (2023), [arXiv:2311.04217 \[cond-mat.str-el\]](https://arxiv.org/abs/2311.04217).
- [42] J. Dong, T. Wang, T. Wang, T. Soejima, M. P. Zaletel, A. Vishwanath, and D. E. Parker, (2023), [arXiv:2311.05568 \[cond-mat.str-el\]](https://arxiv.org/abs/2311.05568).
- [43] T. Soejima, J. Dong, T. Wang, T. Wang, M. P. Zaletel, A. Vishwanath, and D. E. Parker, (2024), [arXiv:2403.05522 \[cond-mat.str-el\]](https://arxiv.org/abs/2403.05522).
- [44] T. Tan and T. Devakul, (2024), [arXiv:2403.04196 \[cond-mat.mes-hall\]](https://arxiv.org/abs/2403.04196).
- [45] Z. Dong, A. S. Patri, and T. Senthil, (2024), [arXiv:2403.07873 \[cond-mat.str-el\]](https://arxiv.org/abs/2403.07873).
- [46] F. D. M. Haldane and E. H. Rezayi, *Phys. Rev. Lett.* **54**, 237 (1985).
- [47] F. C. Zhang, V. Z. Vulovic, Y. Guo, and S. Das Sarma, *Phys. Rev. B* **32**, 6920 (1985).
- [48] E. H. Rezayi and F. D. M. Haldane, *Phys. Rev. B* **32**, 6924 (1985).
- [49] S. M. Girvin, A. H. MacDonald, and P. M. Platzman, *Phys. Rev. Lett.* **54**, 581 (1985).
- [50] S. M. Girvin, A. H. MacDonald, and P. M. Platzman, *Phys. Rev. B* **33**, 2481 (1986).
- [51] M. Kang, A. Pinczuk, B. S. Dennis, M. A. Eriksson, L. N. Pfeiffer, and K. W. West, *Phys. Rev. Lett.* **84**, 546 (2000).
- [52] P. Kumar and F. D. M. Haldane, *Phys. Rev. B* **106**, 075116 (2022).
- [53] D. X. Nguyen, F. D. M. Haldane, E. H. Rezayi, D. T. Son, and K. Yang, *Phys. Rev. Lett.* **128**, 246402 (2022).
- [54] S. A. Brazovskii, *Zh. Eksp. Teor. Fiz.* **68**, 175 (1975).
- [55] Y.-C. Wang, Y. Qi, S. Chen, and Z. Y. Meng, *Phys. Rev. B* **96**, 115160 (2017).
- [56] S. Pu, A. C. Balam, J. Taylor, E. Fradkin, and Z. Papić, (2024), [arXiv:2401.17352 \[cond-mat.str-el\]](https://arxiv.org/abs/2401.17352).
- [57] Y. Xie, A. T. Pierce, J. M. Park, D. E. Parker, E. Khalaf, P. Ledwith, Y. Cao, S. H. Lee, S. Chen, P. R. Forrester, K. Watanabe, T. Taniguchi, A. Vishwanath, P. Jarillo-Herrero, and A. Yacoby,

- [Nature](#) **600**, 439 (2021).
- [58] H. Polshyn, Y. Zhang, M. A. Kumar, T. Soejima, P. Ledwith, K. Watanabe, T. Taniguchi, A. Vishwanath, M. P. Zaletel, and A. F. Young, [Nature Physics](#) **18**, 42 (2022).
- [59] H. Li, U. Kumar, K. Sun, and S.-Z. Lin, [Phys. Rev. Res.](#) **3**, L032070 (2021).
- [60] T. Devakul, V. Crépel, Y. Zhang, and L. Fu, [Nature Communications](#) **12**, 6730 (2021).
- [61] J. Cai, E. Anderson, C. Wang, X. Zhang, X. Liu, W. Holtzmann, Y. Zhang, F. Fan, T. Taniguchi, K. Watanabe, Y. Ran, T. Cao, L. Fu, D. Xiao, W. Yao, and X. Xu, [Nature](#) **622**, 63 (2023).
- [62] H. Park, J. Cai, E. Anderson, Y. Zhang, J. Zhu, X. Liu, C. Wang, W. Holtzmann, C. Hu, Z. Liu, T. Taniguchi, K. Watanabe, J.-H. Chu, T. Cao, L. Fu, W. Yao, C.-Z. Chang, D. Cobden, D. Xiao, and X. Xu, [Nature](#) **622**, 74 (2023).
- [63] Y. Zeng, Z. Xia, K. Kang, J. Zhu, P. Knüppel, C. Vaswani, K. Watanabe, T. Taniguchi, K. F. Mak, and J. Shan, [Nature](#) **622**, 69 (2023).
- [64] F. Xu, Z. Sun, T. Jia, C. Liu, C. Xu, C. Li, Y. Gu, K. Watanabe, T. Taniguchi, B. Tong, J. Jia, Z. Shi, S. Jiang, Y. Zhang, X. Liu, and T. Li, [Phys. Rev. X](#) **13**, 031037 (2023).
- [65] K. Kang, B. Shen, Y. Qiu, K. Watanabe, T. Taniguchi, J. Shan, and K. F. Mak, (2024), [arXiv:2402.03294 \[cond-mat.mes-hall\]](#).
- [66] Z. Lu, T. Han, Y. Yao, A. P. Reddy, J. Yang, J. Seo, K. Watanabe, T. Taniguchi, L. Fu, and L. Ju, [Nature](#) **626**, 759 (2024).
- [67] K. Sun, Z. Gu, H. Katsura, and S. Das Sarma, [Phys. Rev. Lett.](#) **106**, 236803 (2011).
- [68] D. Sheng, Z.-C. Gu, K. Sun, and L. Sheng, [Nature Communications](#) **2**, 389 (2011).
- [69] T. Neupert, L. Santos, C. Chamon, and C. Mudry, [Phys. Rev. Lett.](#) **106**, 236804 (2011).
- [70] N. Regnault and B. A. Bernevig, [Phys. Rev. X](#) **1**, 021014 (2011).
- [71] H. Lu, B.-B. Chen, H.-Q. Wu, K. Sun, and Z. Y. Meng, (2023), [arXiv:2311.15246 \[cond-mat.str-el\]](#).
- [72] A. Weichselbaum, [Annals of Physics](#) **327**, 2972 (2012).
- [73] Q. Niu, D. J. Thouless, and Y.-S. Wu, [Phys. Rev. B](#) **31**, 3372 (1985).
- [74] In this supplemental material, we provide additional ED and DMRG results of the FQAH-FQAHS transition and more details of the the global phase diagram.

**SUPPLEMENTAL MATERIALS FOR
FROM A FRACTIONAL QUANTUM ANOMALOUS HALL STATE TO A SMECTIC STATE WITH EQUAL HALL
CONDUCTANCE**

In the supplementary materials, we provide additional ED and DMRG results of the FQAH-FQAHS transition in Section I and II respectively. In Section III, we show more details of the global phase diagram.

Section I: Supplementary ED results of the FQAH-FQAHS transition

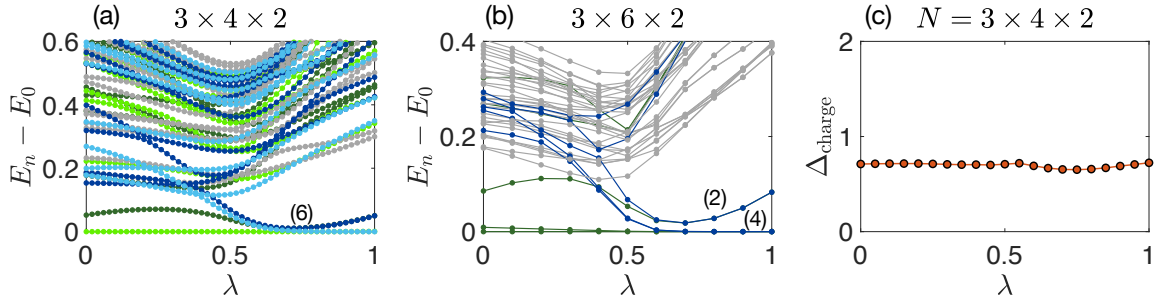


FIG. S1. Here, the simulation path is different from the one introduced in the main text. We define $V_1 = 1.5(1 - \lambda)$, $V_2 = 0.9$, and $V_3 = \lambda$. (a) and (b) show the energy spectra with the change of λ in a $3 \times 4 \times 2$ and a $3 \times 6 \times 2$ torus respectively, and the colors of momentum sectors are defined in Fig.2. The charge gap along the simulated path is shown in (c).

In the main text, we have shown the ED results of the FQAH-FQAHS transition in Fig.2. Here, we show ED results of a different path of this transition, and we define $V_1 = 1.5(1 - \lambda)$, $V_2 = 0.9$, and $V_3 = \lambda$. The energy spectra along the path in a $3 \times 4 \times 2$ and a $3 \times 6 \times 2$ torus are shown in Fig.S1(a,b). When λ is small, the ground state is a FQAH state with 3-fold degeneracy. With the increasing λ , the smectic order is gradually introduced from a perturbation, with another 3 states getting closer to and smoothly converging to the original 3 ground states. In the large λ region, the FQAHS ground states are 6-fold degenerate. In this transition, although the charge-neutral gap is closed at $\lambda \approx 0.6$, the charge gap is not closed as shown in Fig.S1(c). These results are in agreement with our conclusions in the main text.

Section II: Supplementary DMRG results of the FQAH-FQAHS transition

Except the path shown in the main text, we also show another path of this transition from DMRG simulations in a $3 \times 24 \times 2$ cylinder. Here, we consider fixed $V_1 = 1.1$ and $V_2 = 1$, and we change V_3 from 0. With the increasing $\lambda(V_3)$, the smectic order gradually forms as shown in Fig.S2(a). Deep in the FQAH state (small λ), the roton minimum is at (π, π) . When approaching the transition point, the structure factors around (π, π) decrease as shown in Fig.S2(d), while the roton mode at $(\pi, 0)$ goes soft and $S(\pi, 0)$ reaches a peak at critical point as shown in Fig.S2(c), with the bipartite entanglement entropy in Fig.S2(b) goes to a peak as well.

This roton-driven FQAH-FQAHS could be continuous in principle, but the parameter space of critical region and quality of data (especially approaching the critical point) might vary in different paths in the 3 dimensional global phase diagram. We leave the criticality analysis to future work.

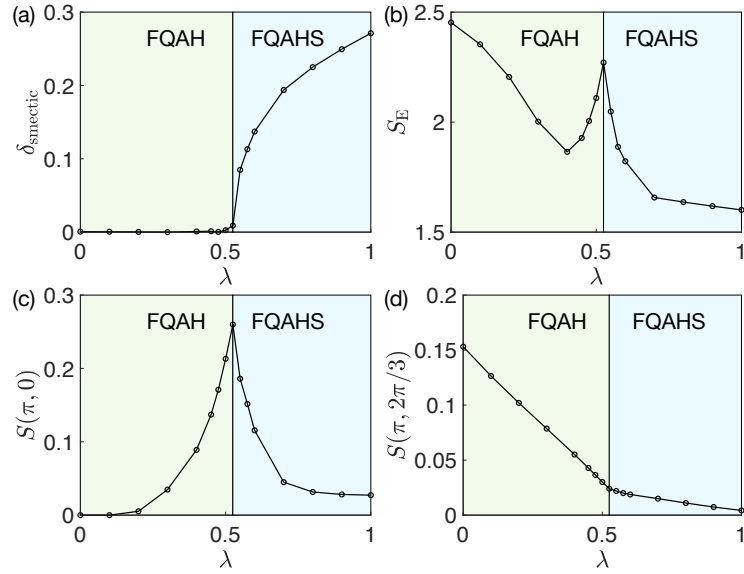


FIG. S2. Here, we fix $V_1 = 1.1$ and $V_2 = 1$, and change $V_3 = \lambda$ only. The change of (a) smectic order parameter, (b) bipartite entanglement entropy, (c) structure factor at $(\pi, 0)$, and (d) structure factor at $(\pi, 2\pi/3)$ are shown along this path in a $3 \times 24 \times 2$ cylinder.

Section III: Supplementary results of the global phase diagram

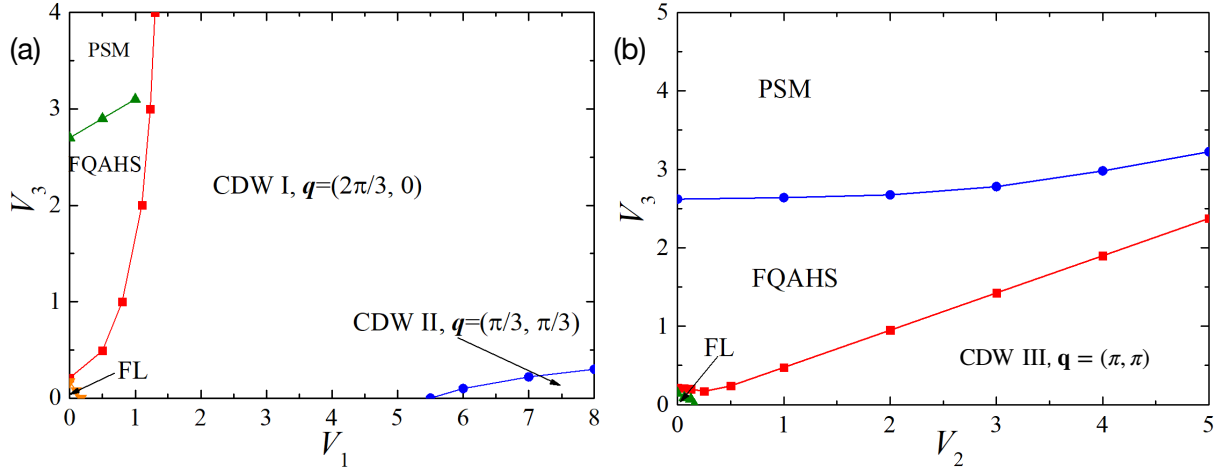


FIG. S3. Supplementary 2 dimensional sections of the 3 dimensional global phase diagram from ED simulations of a $3 \times 4 \times 2$ torus. PSM refers to the polar smectic metal [40]. The CDW I, II, and III states are named in previous work [39].

In previous work, at this filling, the $V_1 - V_2$ phase diagram [39] and the V_3 phase diagram [40] are shown. In this work, 1 dimensional cuts of the 3 dimensional global phase diagram exhibiting the direct FQAH-FQAHS transition are shown. For supplementary information, due to the huge parameter space, we use ED results of a $3 \times 4 \times 2$ torus to show the other 2 dimensional sections: $V_1 - V_3$ in Fig.S3(a) and $V_2 - V_3$ in Fig.S3(b). Some phase boundary in Fig.S3 might suffer from the finite-size effect. For example, the V_1 transition point of the CDW I-CDW II transition is different from the large-scale DMRG results, since the CDW II state has an enlarged unit cell which is not compatible with the $3 \times 4 \times 2$ torus.